

The unique electronic structure of $\text{Ca}_{10}(\text{Pt}_4\text{As}_8)(\text{Fe}_{2-x}\text{Pt}_x\text{As}_2)_5$ with metallic Pt_4As_8 layers

X. P. Shen,¹ S. D. Chen,¹ Q. Q. Ge,¹ Z. R. Ye,¹ F. Chen,² H. C. Xu,¹ S. Y. Tan,¹ X. H. Niu,¹ Q. Fan,¹ B. P. Xie,¹ and D. L. Feng^{1,*}

¹State Key Laboratory of Surface Physics, Department of Physics,
and Advanced Materials Laboratory, Fudan University, Shanghai 200433, People's Republic of China

²Hefei National Laboratory for Physical Science at Microscale and Department of Physics,
University of Science and Technology of China, Hefei, Anhui 230026, People's Republic of China

(Dated: September 15, 2021)

We studied the low-lying electronic structure of the newly discovered iron-platinum-arsenide superconductor, $\text{Ca}_{10}(\text{Pt}_4\text{As}_8)(\text{Fe}_{2-x}\text{Pt}_x\text{As}_2)_5$ ($T_c = 22$ K) with angle-resolved photoemission spectroscopy. We found that the Pt_4As_8 layer contributes to a small electron-like Fermi surface, indicative of metallic charge reservoir layers that are rare for iron based superconductors. Moreover, the electronic structure of the FeAs-layers resembles those of other prototype iron pnictides to a large extent. However, there is only d_{xy} -orbital originated hole-like Fermi surface near the zone center, which is rather unique for an iron pnictide superconductor with relatively high superconducting transition temperature; and the d_{xz} and d_{yz} originated bands are not degenerate at the zone center. Furthermore, all bands near the Fermi energy show negligible k_z dependence, indicating the strong two-dimensional nature of this material. Our results indicate this material possesses rather unique electronic structure, which enriches our current knowledge of iron based superconductors.

PACS numbers: 74.25.Jb, 74.70.-b, 79.60.-i, 71.20.-b

I. INTRODUCTION

The discovery of iron based superconductors with high transition temperature (T_c ; maximally ~ 55 K^{1,2}) has attracted considerable interest. Most iron pnictides have quasi-two dimensional FeAs layers where superconductivity occurs. Extensive experimental and theoretical studies have demonstrated that the low-energy electronic structure of iron pnictides are dominated by multiple Fe-3d orbitals³⁻⁵. The main difference among them lies in the structure of spacer layers between FeAs layers, which mostly contain alkaline metals, alkaline earth metals, rare-earth oxides or alkaline-earth fluorides⁶. These spacer layers serve as “charge reservoirs” as in cuprates and are known to be insulating due to strong ionic bonds. It has been argued that higher T_c of cuprate superconductors are facilitated by enhanced CuO_2 plane coupling through the (Bi,Tl,Hg)-O intermediary layers⁷⁻¹⁰. Then analogous to cuprate, one possible approach for realizing higher T_c in the iron based superconductors is to explore novel spacer layers to tune the electronic states of the FeAs layers^{11,12}.

Recently, superconductivity up to 38 K was reported in the quaternary Ca-Fe-Pt-As system^{13,14}. This system has FeAs layers similar to other iron based superconductors but the spacer layers are composed of two Ca layers and one PtAs layer sandwiched between them. As for PtAs layers, two structures have been identified, Pt_3As_8 and Pt_4As_8 . The two corresponding systems are $\text{Ca}_{10}(\text{Pt}_3\text{As}_8)(\text{Fe}_{2-x}\text{Pt}_x\text{As}_2)_5$ (named as the 10-3-8 compound) and $\text{Ca}_{10}(\text{Pt}_4\text{As}_8)(\text{Fe}_{2-x}\text{Pt}_x\text{As}_2)_5$ (named as the 10-4-8 compound), with maximal $T_c \sim 15$ K¹⁵ and 38 K^{13,14}, respectively. One of the most intriguing features of these materials is that both Pt_nAs_8 ($n=3, 4$) and Fe_2As_2 blocks would compete for the electrons provided by the Ca atoms¹⁶. Based on Zintl's chemical concept, $\text{Ca}_{10}(\text{Pt}_3\text{As}_8)(\text{Fe}_2\text{As}_2)_5$ is a valence satisfied compound with the charges of the $[\text{Pt}_3\text{As}_8]^{10-}$ layer perfectly balanced by the $[\text{Ca}_{10}]^{20+}$ and $[\text{Fe}_{10}\text{As}_{10}]^{10-}$ layers, and thus the Pt_3As_8 layer is expected

to be semiconducting^{13,17}. On the other hand, because of one more Pt atom in the PtAs layer, the $[\text{Pt}_4\text{As}_8]^{12-}$ layer in $\text{Ca}_{10}(\text{Pt}_4\text{As}_8)(\text{Fe}_2\text{As}_2)_5$ is expected to be metallic¹³. The metallic Pt_4As_8 layers would likely enhance the interlayer coupling and might be responsible for the higher T_c as compared to $\text{Ca}_{10}(\text{Pt}_3\text{As}_8)(\text{Fe}_{2-x}\text{Pt}_x\text{As}_2)_5$ ¹⁸. Theoretically, it is proposed that the density of states (DOS) near the Fermi energy (E_F) for both phases has small contributions from the Pt states^{15,19}. However, a recent angle-resolved photoemission spectroscopy (ARPES) study on $\text{Ca}_{10}(\text{Pt}_3\text{As}_8)(\text{Fe}_{2-x}\text{Pt}_x\text{As}_2)_5$ ($T_c = 8$ K) revealed no sign of Fermi pockets from the Pt_3As_8 layer and suggested that the Pt_3As_8 layer couples weakly to the FeAs layer²⁰. Another ARPES study on a 10-3-8 compound ($T_c = 15$ K), and a 10-4-8 compound ($T_c = 35$ K) also does not observe any Fermi pocket from the Pt_3As_8 or Pt_4As_8 layers²¹.

In this article, we present the electronic structure of $\text{Ca}_{10}(\text{Pt}_4\text{As}_8)(\text{Fe}_{2-x}\text{Pt}_x\text{As}_2)_5$ ($T_c = 22$ K), which is an electron overdoped 10-4-8 compound. Our ARPES results reveal an electron Fermi pocket around the zone center of the Pt_4As_8 Brillouin zone (BZ), which makes it the first iron based superconductor with metallic spacer layers. Moreover, all the other bands resembles those of other iron pnictides, and their polarization dependencies indicate that their orbital characters are similar to the corresponding bands in other iron pnictides as well. Furthermore, we have studied the evolution of the band structure along k_z direction in the three-dimensional (3D) momentum space. All bands show negligible k_z dispersion, indicating the pronounced two-dimensionality of this material. Intriguingly, we found that there is only a d_{xy} -originated hole pocket around the Γ -Z or (0,0,0)-(0,0, π) line, which is unique for a iron pnictide superconductor with such a high T_c . The interactions between the Pt_4As_8 layer and the FeAs layer are manifested in the fact that the d_{xz} and d_{yz} originated bands in the FeAs layers are no longer degenerate at Γ . However, we do not observe any folding of the bands in one layer from the umklapp scattering of the crystal field of the other layer, which

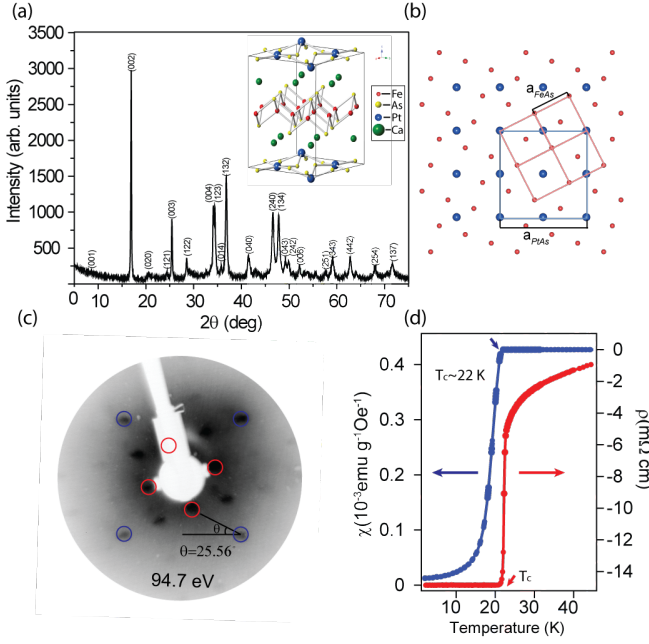


FIG. 1: The crystallographic and superconducting properties of $\text{Ca}_{10}(\text{Pt}_4\text{As}_8)(\text{Fe}_{2-x}\text{Pt}_x\text{As}_2)_5$. (a) Powder XRD pattern of $\text{Ca}_{10}(\text{Pt}_4\text{As}_8)(\text{Fe}_2\text{As}_2)_5$. The powder was obtained by grinding the single crystals. The inset is a schematic picture of the crystal structure of $\text{Ca}_{10}(\text{Pt}_4\text{As}_8)(\text{Fe}_2\text{As}_2)_5$. (b) Top view of Pt_4As_8 and FeAs layers. (c) The Low-energy electron diffraction pattern of a $\text{Ca}_{10}(\text{Pt}_4\text{As}_8)(\text{Fe}_{2-x}\text{Pt}_x\text{As}_2)_5$ single crystal. Reflection peaks from both FeAs (blue circles) and Pt_4As_8 (red circles) lattices are observed. (d) The magnetic susceptibility of an as-grown $\text{Ca}_{10}(\text{Pt}_4\text{As}_8)(\text{Fe}_{2-x}\text{Pt}_x\text{As}_2)_5$ single crystal taken at a magnetic field of 20 Oe in the zero-field cool mode, and its resistivity as a function of temperature.

suggest the interaction is not strong. Our experimental results establish another member of the iron based superconductor family with an unique electronic structure, which enriches our current understanding of these materials. Our results indicate that the charge reservoir layer could alter the electronic structure of iron based superconductors, and the superconducting properties might be enhanced further with novel metallic intermediary layers.

II. SAMPLE PROPERTIES AND EXPERIMENTAL SETUP

Single crystals of $\text{Ca}_{10}(\text{Pt}_4\text{As}_8)(\text{Fe}_{2-x}\text{Pt}_x\text{As}_2)_5$ were synthesized with CaAs , FeAs , Pt powders as starting materials. The mixture with a ratio of $\text{CaAs}:\text{FeAs}:\text{Pt}=1:1:0.5$ was pressed into pellets, loaded into an alumina tube, and then sealed into an argon-filled iron crucible. The entire assembly was heated to 1423 K and kept for 72 h and then slowly cooled down to 1173 K at a rate of 2.5 K/h before shutting off the power. Energy dispersive X-ray spectroscopy (EDX) measurements give a chemical composition of $\text{Ca}:\text{Fe}:\text{Pt}:\text{As}=2:1.905:0.912:3.586$ for an as-grown sample. The ratio between Pt and As is similar to the previous report for another 10-

4-8 compound¹³, but with a higher Pt doping. The X-ray powder diffraction data are shown in Fig. 1(a), which give $a=b=8.731$ Å, and $c=10.537$ Å, similar to those reported in Ref. 13 as well.

The crystal structure of $\text{Ca}_{10}(\text{Pt}_4\text{As}_8)(\text{Fe}_2\text{As}_2)_5$ is shown in the inset of Fig. 1(a), consisting of alternately stacked FeAs and $\text{Ca-Pt}_4\text{As}_8\text{-Ca}$ layers¹³. In contrast to the “111”, “122” prototype iron pnictides, it has an additional Pt_4As_8 layer between the two Ca layers, and the distance between the neighboring FeAs layer is among the largest in iron pnictides. Note that, the Ca atoms and the FeAs layers are arranged in the similar tetragonal structure to the “111” iron pnictides, while the unique Pt_4As_8 layer matches the FeAs lattice constant with $a_{\text{PtAs}}=\sqrt{5} a_{\text{FeAs}}$ and a rotation of $\theta=25.56^\circ$ [Fig. 1(b)], which is clearly shown by low energy electron diffraction (LEED) pattern in Fig. 1(c). Consequently, the unit cell of $\text{Ca}_{10}(\text{Pt}_4\text{As}_8)(\text{Fe}_2\text{As}_2)_5$ is tetragonal.

Magnetic susceptibility measurements were performed with Quantum Design superconducting quantum interference device (SQUID) and in-plane resistivity measurements were performed with a Quantum Design physical property measurements system (PPMS). With Pt partially substituted for Fe in the FeAs layer in our as-grown $\text{Ca}_{10}(\text{Pt}_4\text{As}_8)(\text{Fe}_{2-x}\text{Pt}_x\text{As}_2)_5$ sample, resistivity and magnetic susceptibility measurements show clear signature of a superconducting transition at $T_c=22$ K [Fig. 1(d)]. The narrow transition temperature width demonstrates the high quality of the $\text{Ca}_{10}(\text{Pt}_4\text{As}_8)(\text{Fe}_{2-x}\text{Pt}_x\text{As}_2)_5$ crystals.

ARPES measurements were performed at (1) Beamline 7U of the UVSOR synchrotron facility, with a variable photon energy and MBS A-1 electron analyzer, (2) the surface and interface spectroscopy Beamline of the Swiss Light Source (SLS), and (3) at an in-house system equipped with an SPECS UVLS helium discharging lamp. Scienta electron analyzers are equipped in the (2) and (3) setups. The overall energy resolution was set to 15 meV or better, and the typical angular resolution was 0.3° . The samples were pre-oriented by Laue diffraction, cleaved *in situ* and then measured under ultrahigh vacuum better than 6×10^{-11} mbar. The experimental setup for polarization-dependent ARPES is shown in Fig. 2(a). The incident beam and the sample surface normal define a mirror plane. For the *s* (or *p*) experimental geometries, the electric field of the incident photons is out of (or in) the mirror plane. The matrix element for the photoemission process could be described as

$$|M_{f,i}^{\mathbf{k}}|^2 \propto |\langle \Psi_f^{\mathbf{k}} | \hat{\epsilon} \cdot \mathbf{r} | \Psi_i^{\mathbf{k}} \rangle|^2$$

Since the final state $\Psi_f^{\mathbf{k}}$ of photoelectrons could be approximated by a plane wave with its wave vector in the mirror plane, $\Psi_f^{\mathbf{k}}$ is always even respect to the mirror plane in our experimental geometry. In the *s* (or *p*) geometry, $\hat{\epsilon} \cdot \mathbf{r}$ is odd (or even) with respect to the mirror plane. Thus considering the spatial symmetry of the 3d orbitals, when the analyzer slit is along the high-symmetry directions, the photoemission intensity of specific even (or odd) component of a band is only detectable with the *p* (or *s*) polarized light. For example, with respect to the mirror plane (the *xz* plane), the even orbitals

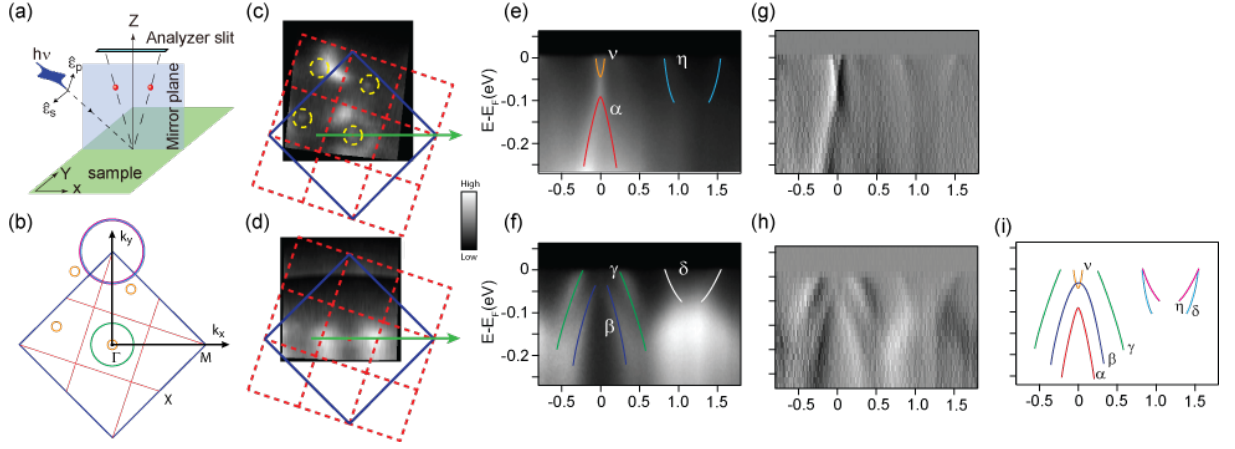


FIG. 2: Photoemission data of $\text{Ca}_{10}(\text{Pt}_4\text{As}_8)(\text{Fe}_{2-x}\text{Pt}_x\text{As}_2)_5$. (a) Schematic of two polarization geometries of experimental setups, reproduced from Ref.²⁴. (b) Sketch of Fermi surface for $\text{Ca}_{10}(\text{Pt}_4\text{As}_8)(\text{Fe}_{2-x}\text{Pt}_x\text{As}_2)_5$. (c) Photoemission intensity map at the Fermi energy (E_F) integrated over $[E_F-10 \text{ meV}, E_F+10 \text{ meV}]$ in p polarization. The 2D Brillouin zone in blue is for FeAs layer and the dash one in red is for PtAs layer. (e) Photoemission intensity along $(0, 0)-(\pi, 0)$ direction, as indicated by the green arrow in panel a. The solid lines indicate the bands dispersions extracted from the corresponding MDC's. (g) The second derivative with respect to energy of the data in panel a. (d), (f), and (h) are the same as in panels c, e, and g, respectively, but taken in s polarization. (i) Summary of the experimental band structure for $\text{Ca}_{10}(\text{Pt}_4\text{As}_8)(\text{Fe}_{2-x}\text{Pt}_x\text{As}_2)_5$. All data were taken with 26 eV photons at UVSOR.

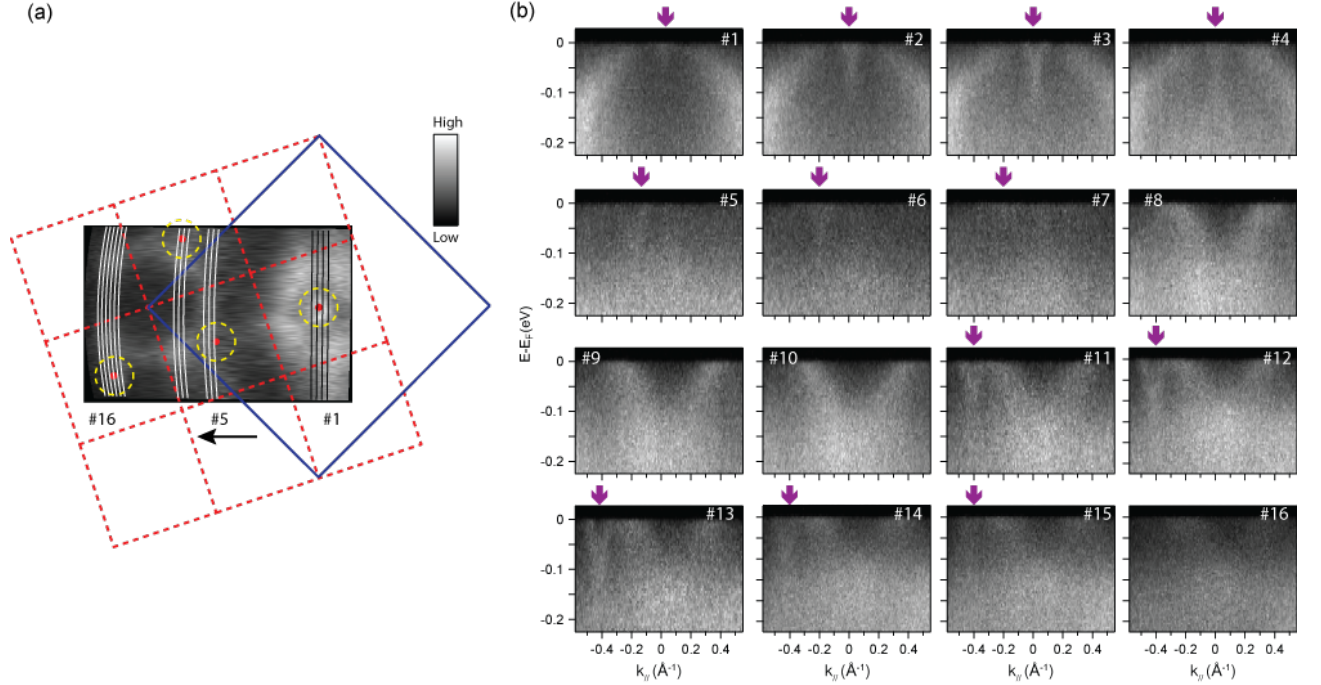


FIG. 3: Photoemission data of $\text{Ca}_{10}(\text{Pt}_4\text{As}_8)(\text{Fe}_{2-x}\text{Pt}_x\text{As}_2)_5$. (a) Photoemission intensity map at E_F integrated over $[E_F-30 \text{ meV}, E_F+30 \text{ meV}]$. The small electron pockets are enclosed by the dash circles. (b) Photoemission intensity plots of cuts #1-#16 as indicated in panel a. The positions of the small electron pockets are marked by the arrows. All data were taken with randomly polarized 21.2 eV photons from a helium discharge lamp.

(d_{xz} , d_{z^2} , and $d_{x^2-y^2}$) and the odd orbitals (d_{xy} and d_{yz}) could be only observed in the p and s geometries, respectively^{22,23}.

III. EXPERIMENTAL RESULTS AND ANALYSES

The photoemission intensity maps in the p and s polarizations are shown in Figs. 2(c) and 2(d), respectively. As summarized in Fig. 2(b), the observed Fermi surface consists of one hole pocket and one electron pocket around the zone

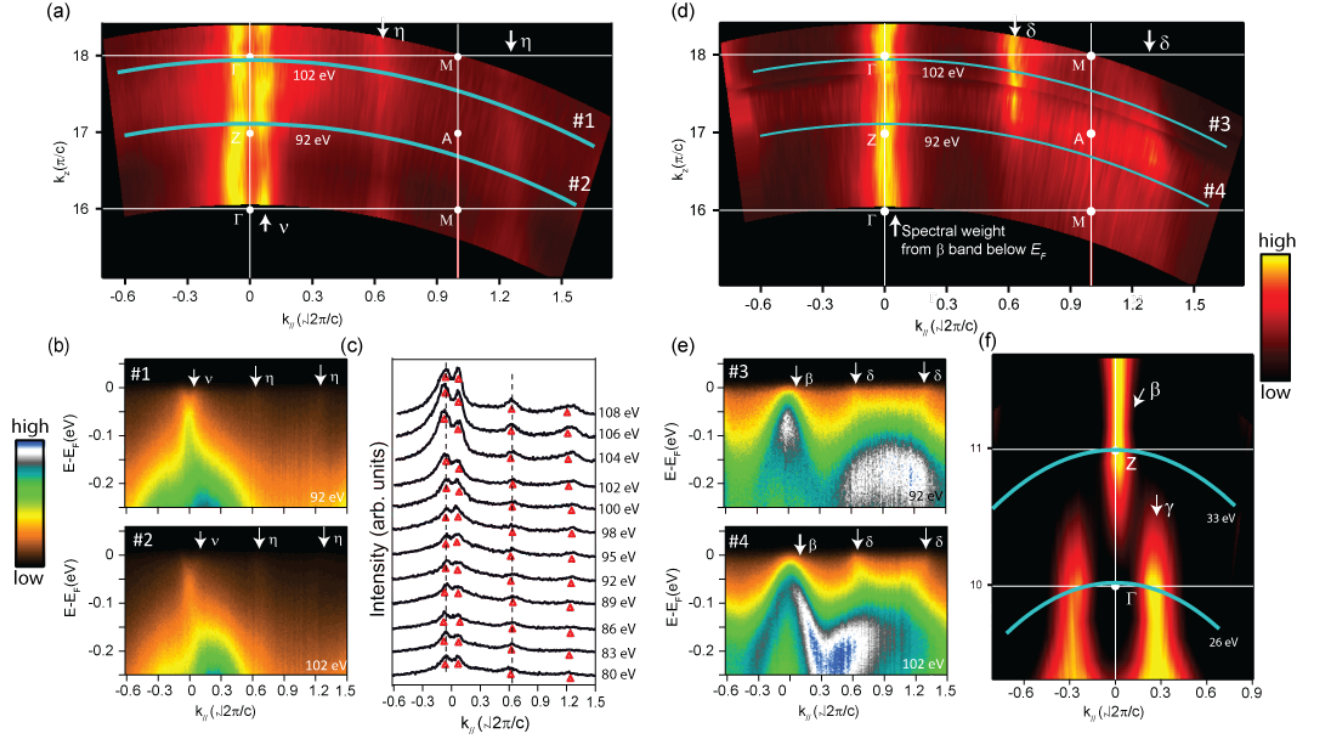


FIG. 4: The Fermi surface and band structure as a function of k_z for $\text{Ca}_{10}(\text{Pt}_4\text{As}_8)(\text{Fe}_{2-x}\text{Pt}_x\text{As}_2)_5$. (a) Photoemission intensity map in the k_x - k_z plane in p polarization. (b) The photoemission intensity with typical photon energies along the cuts #1 and #2 in panel a. (c) The corresponding MDC's at E_F with different photon energies in panel a, the peaks indicating Fermi crossing k_F are marked by red solid triangles. (d)-(e) are the same as in panels a-b, respectively, but in s polarization. (f) is the same as in panel d, but taken at low photon energies from 22 eV to 38 eV for a better momentum resolution. Different k'_z 's were accessed by varying the photon energies at Beamline of SLS and Beamline 7U of UVSOR, as indicated by the blue lines, where an inner potential of 13 eV is used to obtain k_z . The data in panels (a-e) and panel (f) were collected at SLS and UVSOR, respectively.

center, two electron pockets around the zone corner of the FeAs BZ, as well as several electron pockets located around the zone centers of extended Pt_4As_8 BZs. For simplicity, we will use the BZ according to the tetragonal FeAs lattice hereafter, if not specified. The photoemission intensity along $(0, 0) - (\pi, 0)$ under the p and s geometries are further displayed in Figs. 2(e) and 2(f), respectively. Around the zone center, an electron band assigned as ν together with a fast dispersive band α below ~ 90 meV is resolved in the p polarization. The ν band crosses E_F , forming a small electron pocket. On the other hand, two bands (β and γ) show up in the s polarization. The γ band crosses E_F , forming a hole pocket around the zone center, while the band top of β is about 35 meV below E_F . With the assistance from the second derivative of the photoemission intensity with respect to energy, two electron bands around the zone corner, η and δ , are clearly identified in p and s geometries respectively, exhibiting opposite spatial symmetries.

In general, as recapitulated in Fig. 2(i), most of the bands resemble the band structures in the prototype iron pnictides except the electron-like band (ν) around the zone center, which demonstrates that the low-lying electronic structures of $\text{Ca}_{10}(\text{Pt}_4\text{As}_8)(\text{Fe}_{2-x}\text{Pt}_x\text{As}_2)_5$ are mainly from the Fe-3d orbitals. Moreover, the polarization dependencies for these bands are the same as those in NaFeAs and other iron pnictides.

Therefore, according to previous knowledge on iron pnictides^{22,23}, we can ascribe their orbital characters along the $\Gamma - M$ direction as follow:

1. α around the zone center could be ascribed to the even d_{xz} orbital;
2. β could be ascribed to the odd d_{yz} orbital;
3. γ could be ascribed to the d_{xy} orbital;
4. δ around the zone corner could be ascribed to the d_{xy} orbital;
5. η could be ascribed to the d_{xz} orbitals.

Despite the overall similarity, there are still obvious differences between the Fermi surface sheets of $\text{Ca}_{10}(\text{Pt}_4\text{As}_8)(\text{Fe}_{2-x}\text{Pt}_x\text{As}_2)_5$ and those of the prototype iron pnictides. First of all, the band tops of the d_{xz} dominated α band and the d_{yz} dominated β band are not degenerate at Γ (Fig. 2(i)). This means that the rotational symmetry of the tetragonal FeAs layer is broken, which might be due to the crystalline potential imposed by the Pt_4As_8 layer. Secondly, besides the small ν electron pocket around Γ , several bright features are further observed, as enclosed by dash lines in Fig. 2(a). These features are more obvious in the data taken

with randomly polarized 21.2 eV photons in Fig. 3, where four small electron pockets are observed and they match well with the BZs of Pt_4As_8 layer. The momentum evolution of the electron pockets are revealed by the photoemission intensity plots in Fig. 3(b), particularly along the cuts #1-#4 and #11-#16. The dispersions of these electron-like bands are identical as expected. Based on these observations, the ν Fermi pocket should be attributed to the states in the Pt_4As_8 layer. This finding qualitatively agrees with a recent first principles band calculation¹⁹, which suggests that the Pt_4As_8 layers contribute to small electron-like bands at the zone center.

To understand the detailed electronic structure evolution along k_z direction in 3D momentum space, the photon energy dependent ARPES measurements were conducted. The measured Fermi surface cross-section in the k_x - k_z plane for both p and s polarizations are shown in Figs. 4(a) and 4(d), respectively. The cross-sections of the ν , η and δ Fermi surfaces are nearly straight cylinders along k_z direction, thus indicating weak k_z dependence. Note that in Fig. 4(d), the strong spectral weight around zone center originates from the band top of β below E_F and the γ band is hardly visible, likely due to matrix element effects. As shown in Fig. 4(f), the γ band is better revealed at lower photon energies and negligible k_z dispersion is observed. Therefore, all bands show negligible k_z dispersion, indicating the strong two-dimensional (2D) nature of the electronic states. The two dimensional nature is an expected consequence of the thick $\text{Ca-Pt}_4\text{As}_8\text{-Ca}$ spacer layer between the neighboring two FeAs layers, and similar experimental results were observed in LaOFeAs ²⁴. Moreover, we note that there is an ellipsoidal electron Fermi surface around Z in heavily electron doped iron pnictides such as $\text{LiFe}_x\text{Co}_{1-x}\text{As}$ or $\text{NaFe}_x\text{Co}_{1-x}\text{As}$ ²⁵, the negligible k_z dispersion of ν here again shows that it is from the Pt_4As_8 layer.

IV. DISCUSSIONS AND CONCLUSIONS

Based on the above analysis, the most unique electronic structure of the 10-4-8 compound studied here is its electron pocket around zone center of the Pt_4As_8 BZ, which makes it the first experimentally proven iron pnictide whose spacer layer is metallic and likely participates in superconductivity. The recent ARPES measurements of another 10-4-8 compound ($T_c=35$ K) did not find such an electron pocket²¹. Based on the Fermi surface volume, it is clear that our sample is doped with more electrons. Moreover, since Fermi surface originated from the Pt_3As_8 layer has never been observed for the 10-3-8 compounds with much lower T_c ^{20,21}, the metallicity of the spacer layer might not be so relevant to the superconductivity in these Ca-Fe-Pt-As compounds. On the other hand, due to proximity effect, the superconductivity in the FeAs layer will also result in superconductivity in the Pt_4As_8 layer. The pairing behaviors on the ν pocket deserves further investigation, and we leave this for the future studies.

When considering the impact of Pt_4As_8 layer on FeAs

layer, we notice that the d_{xz}/d_{yz} orbital is no longer equivalent and are not degenerate at Γ . This suggests that the crystalline potential arising from Pt_4As_8 layer breaks the rotational symmetry of FeAs tetragonal lattice. On the other hand, the crystalline potential of the Pt_4As_8 or FeAs layer does not cause any observable umklapp scattering, which would result in band folding²⁶. However, we notice that such a non-degenerate behavior of the d_{xz}/d_{yz} bands was observed in a 10-3-8 compound but not in a 10-4-8 compound²¹. This disagreement might be due to some sample-specific issues that needs further exploration.

The electronic structure of the FeAs-layer in this 10-4-8 compound ($T_c=22$ K) is somewhat similar to that of LiFeAs ²⁵, which has only one large hole-like Fermi surface pockets made of the d_{xy} orbital around Γ . However for LiFeAs , there is a hole Fermi pocket made of d_{xz}/d_{yz} orbitals around Z, which was considered to be crucial for the superconductivity. It was found that the superconductivity disappears following the disappearance of the d_{xz}/d_{yz} -based small hole-like Fermi pocket with increased cobalt doping. Meanwhile, the d_{xy} -based band was found to be heavily scattered by the cobalt impurity²⁵, which might explain why it could not sustain the superconductivity. Similar behaviors have been found in $\text{BaFe}_{2-x}\text{Co}_x\text{As}_2$ as well²⁷, where the d_{xy} -based hole Fermi surface was considered not to be able to sustain the superconductivity. In contrast, although there is only d_{xy} -based hole like Fermi surface in the 10-4-8 compound studied here, its T_c is still relatively high, which is in coherence with its relatively small scattering rate. Such an iron pnictide superconductors with only a d_{xy} -based hole Fermi surface at the zone center is rather unique.

To summarize, we have reported the electronic structure of $\text{Ca}_{10}(\text{Pt}_4\text{As}_8)(\text{Fe}_{2-x}\text{Pt}_x\text{As}_2)_5$ by ARPES and resolved a rather unique Fermi surface topology. Its electronic structure is rather two-dimensional due to its unusually thick spacer layer. We have observed the Fermi surface of the Pt_4As_8 layer, which makes it the first iron based superconductor with metallic spacer layers. The Fermi surfaces of the FeAs layers show good correspondence to those of other prototype iron pnictides, except there is only a d_{xy} -based hole Fermi cylinder. Our data thus establish an unique iron based superconductor with a particular electronic structure, which deepens and enriches the current understanding of these materials.

V. ACKNOWLEDGEMENTS

Part of this work was performed at the Surface and Interface Spectroscopy Beamline, SLS, Paul Scherrer Institute, Villigen, Switzerland and Beamline 7U of the UVSOR synchrotron facility, Institute for Molecular Science and The Graduate University for Advanced Studies, Okazaki, Japan. This work is supported by the National Basic Research Program of China (973 Program) under the grant Nos. 2012CB921402, 2011CB921802, 2011CBA00112, and National Science Foundation of China.

-
- * Electronic address: dlfeng@fudan.edu.cn
- ¹ Z. A. Ren, W. Lu, J. Yang, W. Yi, X. L. Shen, Z. C. Li, G. C. Che, X. L. Dong, L. L. Sun, F. Zhou, and Z. X. Zhao, *Chin. Phys. Lett.* **25**, 2215 (2008).
 - ² H. Kito, H. Eisaki, and A. Iyo, *J. Phys. Soc. Jpn.* **77**, 063707 (2008).
 - ³ K. Kuroki, S. Onari, R. Arita, H. Usui, Y. Tanaka, H. Kontani, and H. Aoki, *Phys. Rev. Lett.* **101**, 087004 (2008).
 - ⁴ Y. Ran, F. Wang, H. Zhai, A. Vishwanath, and D.H. Lee, *Phys. Rev. B* **79**, 014505 (2009).
 - ⁵ S. Graser, T. A. Maier, P. J. Hirschfeld, and D. J. Scalapino, *New J. Phys.* **11**, 025016 (2009).
 - ⁶ M. Nohara, S. Kakiya, K. Kudo, Y. Oshiro, S. Araki, T. C. Kobayashi, K. Oku, E. Nishibori, H. Sawa, *Solid State Commun.* **152**, 635-639 (2003).
 - ⁷ P. A. Sterne and C. S. Wang, *J. Phys. C: Solid State Phys.* **21**, 949 (1988).
 - ⁸ Z. Z. Sheng, A. M. Hermann, A. El Ali, C. Almasan, J. Estrada, T. Datta, and R. J. Matson, *Phys. Rev. Lett.* **60** 937 (1988).
 - ⁹ S. S. P. Parkin, V. Y. Lee, E. M. Engler, A. I. Nazzal, T. C. Huang, G. Gorman, R. Savoy, and R. Beyers, *Phys. Rev. Lett.* **60** 2539 (1988).
 - ¹⁰ L. Gao, Z. J. Huang, R. L. Meng, J. G. Lin, F. Chen, L. Beauvais, Y. Y. Sun, Y. Y. Xue, C. W. Chu, *Physica C* **213**, 261 (2012).
 - ¹¹ X. Y. Zhu, F. Han, G. Mu, P. Cheng, B. Shen, B. Zeng, and H. H. Wen, *Phys. Rev. B* **79**, 220512 (2009).
 - ¹² P. M. Shirage, K. Kihou, C. H. Lee, H. Kito, H. Eisaki, and A. Iyo, *J. Am. Chem. Soc.* **133**, 9630 (2011).
 - ¹³ N. Ni, J. M. Allred, B. C. Chan, and R. J. Cava, *Proc. Natl. Acad. Sci. USA* **108**, E1019 (2011).
 - ¹⁴ S. Kakiya, K. Kudo, Y. Nishikubo, K. Oku, E. Nishibori, H. Sawa, T. Yamamoto, T. Nozaka, and M. Nohara, *J. Phys. Soc. Jpn.* **80**, 093704 (2011).
 - ¹⁵ C. Lönert, T. Stürzer, M. Tegel, R. Frankovsky, G. Friederichs, D. Johrendt, *Angew. Chem. Int. Ed.* **50**, 9195-9199, (2011).
 - ¹⁶ T. Stürzer, G. Derondeau, and D. Johrendt, *Phys. Rev. B* **86**, 060516 (2012).
 - ¹⁷ J. Willem and G. Bos, *Annu. Rep. Prog. Chem., Sect. A: Inorg. Chem* **108**, 408C423, (2012).
 - ¹⁸ I. R. Shein and A. L. Ivanovskii, *Theor. Exp. Chem.* **47**, 292 (2011).
 - ¹⁹ H. Nakamura and M. Machida, *Physica C* **484**, 39 (2012).
 - ²⁰ M. Neupane, C. Liu, S. Y. Xu, Y. J. Wang, N. Ni, J. M. Allred, L. A. Wray, N. Alidoust, H. Lin, R. S. Markiewicz, A. Bansil, R. J. Cava, and M. Z. Hasan, *Phys. Rev. B* **85**, 094510 (2012).
 - ²¹ S. Thirupathaiah, T. Stürzer, V. B. Zabolotnyy, D. Johrendt, B. Büchner, and S. V. Borisenko, *arXiv:1307.16082v1*.
 - ²² Y. Zhang, F. Chen, C. He, B. Zhou, B. P. Xie, C. Fang, W. F. Tsai, X. H. Chen, H. Hayashi, J. Jiang, H. Iwasawa, K. Shimada, H. Namatame, M. Taniguchi, J. P. Hu, and D. L. Feng, *Phys. Rev. B* **83**, 054510 (2011).
 - ²³ Y. Zhang, C. He, Z. R. Ye, J. Jiang, F. Chen, M. Xu, Q. Q. Ge, B. P. Xie, J. Wei, M. Aeschlimann, X. Y. Cui, M. Shi, J. P. Hu, and D. L. Feng, *Phys. Rev. B* **85**, 085121 (2012).
 - ²⁴ L. X. Yang, B. P. Xie, Y. Zhang, C. He, Q. Q. Ge, X. F. Wang, X. H. Chen, M. Arita, J. Jiang, K. Shimada, M. Taniguchi, I. Vobornik, G. Rossi, J. P. Hu, D. H. Lu, Z. X. Shen, Z. Y. Lu, and D. L. Feng, *Phys. Rev. B* **82**, 104519 (2010).
 - ²⁵ Z. R. Ye, Y. Zhang, M. Xu, Q. Q. Ge, Q. Fan, F. Chen, J. Jiang, P. S. Wang, J. Dai, W. Yu, B. P. Xie, and D. L. Feng, *arXiv:1303.0682v1*.
 - ²⁶ H. W. Ou, J. F. Zhao, Y. Zhang, B. P. Xie, D. W. Shen, Y. Zhu, Z. Q. Yang, J. G. Che, X. G. Luo, X. H. Chen, M. Arita, K. Shimada, H. Namatame, M. Taniguchi, C. M. Cheng, K. D. Tsuei, and D. L. Feng, *Phys. Rev. Lett.* **102** 026806 (2009).
 - ²⁷ C. Liu, T. Kondo, R. M. Fernandes, A. D. Palczewski, E. D. Mun, N. Ni, A. N. Thaler, A. Bostwick, E. Rotenberg, J. Schmalian, S. L. Budko, P. C. Canfield, and A. Kaminski, *Nature Phys.* **6** 419 (2010).